IEEE Access
Multidisciplinary | Rapid Review | Open Access Journal

Received April 25, 2019, accepted May 13, 2019, date of publication May 28, 2019, date of current version June 27, 2019.

Digital Object Identifier 10.1109/ACCESS.2019.2919518

Polarization-Reconfigurable and Frequency-Tunable Dipole Antenna Using Active AMC Structures

DONGXU CHEN[1], (Student Member, IEEE), WANCHEN YANG[1,2], (Member, IEEE), WENQUAN CHE[1,2], (Senior Member, IEEE), QUAN XUE[2], (Fellow, IEEE), AND LIZHENG GU[1], (Student Member, IEEE)

[1]Department of Communication Engineering, Nanjing University of Science and Technology, Nanjing 210094, China
[2]School of Electronic and Information Engineering, South China University of Technology, Guangzhou 510641, China

Corresponding author: Wenquan Che (eewqche@scut.edu.cn)

This work was supported in part by the Guangdong Innovative and Entrepreneurial Research Team Program under Grant 2017ZT07X032, in part by the National Natural Science Foundation of China under Grant 61571231 and Grant 61601224, and in part by the Natural Science Foundation of Jiangsu Province under Grant BK20160844.

ABSTRACT A polarization-reconfigurable and frequency-tunable mechanism based on an active artificial magnetic conductor (AMC) structure is proposed. The active AMC unit cell consists of a four-corner-cut inner patch and four triangles loaded with four varactors, and it can realize polarization-reconfigurable and frequency-tunable reflection characteristics by adjusting the capacitance of the varactors. By employing it as a ground plane of a pair of linearly-polarized dipole antennas, a multi-functional antenna can be well designed with polarization reconfigurability and frequency-tuning capability. By controlling the DC bias of the varactors accordingly, the three polarization states of right-/left-handed circular polarization (R/LHCP) and linear polarization (LP) can be switched, respectively, while the operating frequency of each polarization can be flexibly tuned. The measured tuning frequency ratio for the LP state ($|S_{11}| < -10$dB) can reach 1.56:1, while the ratio for either the LHCP or RHCP state (axial ratio$<$ 3dB) is about 1.28:1. Moreover, a large bandwidth for each polarization state can be obtained, where the bandwidths are up to 17.1% and 8.7%, respectively, for the LP and CP states. Besides, it is more flexible for the CP states since the bandwidth can be adjusted. For a demonstration, one prototype of the proposed antenna is fabricated and measured. The agreement between the theoretical and measured results indicates good performances of the proposed antenna.

INDEX TERMS Artificial magnetic conductor (AMC), broadband, frequency-tunable, multi-functional antenna, polarization-reconfigurable.

I. INTRODUCTION

In recent years, owing to the development of multifunction requirements in wireless and satellite communication systems, reconfigurable antennas are required to fulfill these demands including frequency tunability, polarization reconfigurability, radiation pattern beam switching control, or their combinations [1]–[4]. Among them, multi-polarization systems are extremely attractive due to their features of channel fading immunity, communication reliability enhancement, and channel capacity improvement [5], [6]; while the frequency-tunable antennas also arouse a lot of research interests since they can allow frequency hopping and dynamic spectrum allocation [7].

The associate editor coordinating the review of this manuscript and approving it for publication was Lin Peng.

So far, many researches have been carried out on the antennas with single reconfigurability. For example, the most common multi-polarization approach is to change the path of currents on antenna through electrically controllable switches, and different polarization states can thus be obtained by controlling the ON/OFF status of the switches, such as loading switches in the slot antennas [8] or the slots [9], [10] on the patch antennas or ground plane [11]. The merit of this method is its simplicity, but the 3-dB axial ratio (AR) bandwidth for circular polarization (CP) of such patch or slot antennas are very small (<5%). In contrast, the dipole antennas with four pin-diodes [12] can achieve larger CP bandwidth over 10%, with a relatively larger height of $0.25\lambda_0$. Another method is utilizing a reconfigurable feeding network to change the phase differences between multi-feeding points for multi-fed antennas [6], [13]–[15].

However, most of these works suffer from the bulky feeding network and RF insertion loss, which would lead to a negative effect on antenna gain and system noise temperature and thus fail to meet the compact requirement. Moreover, for the frequency-reconfigurable antennas, simple methods using PIN diode switches at specific locations to change the effective electrical length and hence forming different resonance frequencies have been proposed in [1], [16].

Aiming at improving the reconfiguration capabilities, further researches on multi-parameter reconfigurations have been carried out. In [17], a microstrip antenna with frequency agility and polarization diversity was realized by loading several RF switches and tuning diodes in the feed network to respectively provide four polarization states, and tune the antenna center frequency across a large tunable frequency ratio of 1.4:1. A novel cavity-backed slot antenna [18] was capable of reconfiguring the frequency, polarization, and radiation pattern by electronically controlling the state of switches between two crossed slots etched on the surfaces of a substrate integrated waveguide cavity. In addition, a magneto-electric (ME) dipole antenna [5] can provide four polarization states and is switchable in two adjacent frequency bands. But above-mentioned works normally exhibit very small working bandwidth (<5%) for each state, and only two or three tuning bands were realized by using limited states of the switches. However, for modern wireless communication systems, wideband communication is also becoming a trend to meet the demands of high rate and large capacity. Therefore, how to achieve a flexible broadband multi-reconfigurable antenna is still a big challenge.

As we know, metamaterial [19], [20] has been widely used in various antenna designs due to the distinctive EM reflection properties for certain incident waves. Recently, metamaterials have been used to realize high-performance reconfigurable antennas with multiple polarizations [21], [22] or frequencies [23], [24], as well as multi-reconfigurability antennas [25]–[27]. In [25], a dual-layer electromagnetic band gap (EBG) structure was employed as the ground plane of a monopole antenna. By tuning the bias voltages across the varactors in the EBG cells, frequency-tunable right-/left-handed CP (R/LHCP) performances can be achieved with a tunable bandwidth of 40% for AR< 3dB. However, the DC biasing is too complicated because of the dual-layer EBG structure. In [26], a tunable artificial magnetic conductor (AMC) substrate combined with tunable crossed end-loaded dipoles was designed to realize nearly arbitrary polarizations including frequency-tunable R/LHCP and LP states with various orientations. In [27], a pixel surface was used as a parasitic layer to provide reconfiguration capabilities to existing antennas, then reconfigurable frequency, radiation pattern and polarization with a tuning range about 25% were realized. However, in these works, the bandwidth at single CP state is very small (< 3.4%) and many performances (such as gain, radiation pattern or AR bandwidth, etc.) were not investigated.

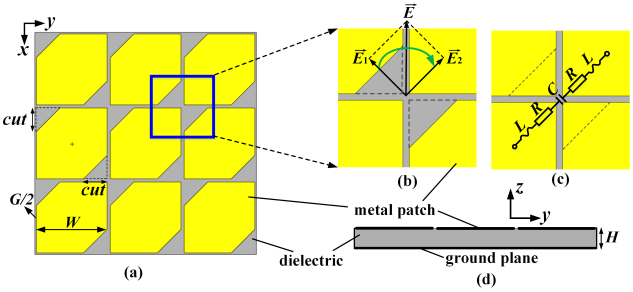

FIGURE 1. (a) top view of the corner-cut PRAMC structure (b) zoom-in view of the corner-cut PRAMC, (c) AMC unit cell without truncation and (d) side view of the corner-cut PRAMC. (W = 18 mm, G = 0.2 mm, cut = 9 mm, H = 5mm).

In this paper, to realize a low-profile multi-functional antenna, a novel active AMC structure with different polarizations and tunable reflection characteristics in a wide frequency range is proposed. By controlling the DC bias of the loaded varactors appropriately, the AMC-based antenna can not only take the reconfigurable polarization states (R/LHCP and LP), but also take tunable operating frequency at each polarization state. Moreover, large tuning frequency ratios, large AR bandwidths for CP states, and wide impedance bands for LP states can also be achieved. This paper is organized as follows. In Section II, the design principle of the active AMC and its wideband tuning characteristics are introduced. Next, one broadband multi-functional antenna based on the active AMC structure is designed and its performance is investigated in Section III. Finally, the proposed antenna is fabricated and measured for demonstration in Sections IV.

II. POLARIZATION-RECONFIGURABLE AND FREQUENCY-TUNABLE ACTIVE AMC STRUCTURE

A. CORNER-CUT POLARIZATION-ROTATION AMC (PRAMC) STRUCTURE

To realize a multi-functional AMC structure, a corner-cut polarization-rotation AMC (PRAMC) structure based on the previously reported polarization-rotation technique [21] is firstly constructed and analyzed, as shown in Fig. 1. It consists of a top dual-corner-cut metal patch, a supporting substrate and a ground plane. The two truncated corners are located along the +45° diagonal direction, where the surface impedance would be substantially changed and much different from that along the -45° direction, thus resulting in 90° polarization rotation of incident waves. Here, the substrate is a FR4 slab (ε_r = 4.4, $tan\ \delta$ = 0.02). All the dimensions are listed in Fig. 1.

For better understanding, the equivalent circuit of the corner-cut PRAMC surface is also given in Fig. 1(b)-(c) according to [21]. Suppose that a TM plane wave with -x-direction electric field is perpendicularly incident on the PRAMC surface. Suppose that the E-field is developed along the x-axis, and resolve it into two orthogonal components along the ± 45°, as shown in Fig. 1(b). As we know, for the AMC unit cell without truncation (see Fig. 1(c)), the RLC circuit of the orthogonal components $\vec{E_1}$ and $\vec{E_2}$ is identical

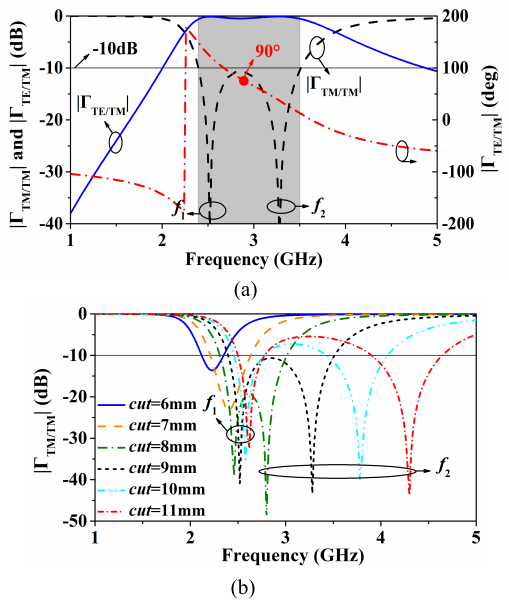

FIGURE 2. The dyadic reflection coefficients of the PRAMC structures in cases of (a) *cut* = 9 mm and (b) *cut* = 6 ∼ 11 mm.

because of the symmetrical structure and the impedance can be calculated by

$$Z = 2R + jw(2L) + \frac{1}{jwc} = R' + jX' \tag{1}$$

where R and L are the inductance and resistance of each patch, respectively, C is the capacitance created by the gaps between adjacent and opposite patches. However, for the AMC unit with corner-truncations, the impedance of the $\overrightarrow{E_1}$ and $\overrightarrow{E_2}$ would be different, which can be given respectively as

$$Z_1 = R'_1 + jX'_1 \tag{2}$$

$$Z_2 = R'_2 + jX'_2 \tag{3}$$

Here, X'_1 is larger than X'_2 since the corners are truncated to widen the gaps between the adjacent and opposite patches. Thus, the sizes of the truncated corners *cut* can be used to vary the phase difference between Z_1 and Z_2. If $|Z_1| = |Z_2|$ and $\angle Z_1 - \angle Z_2 = 90°$ then $\left|\overrightarrow{E_1}\right| = \left|\overrightarrow{E_2}\right|$ and $\angle\overrightarrow{E_1} - \angle\overrightarrow{E_2} = 90°$, and thus RHCP can be obtained (see Fig. 1(b)).

Furtherly, the polarization-rotation property of the corner-cut PRAMC is also investigated by Floquet-port Model. Suppose that a TM plane wave with x-direction electric field is perpendicularly incident on the PRAMC surface. $\Gamma_{TE/TM}$ is used to represent the ratio of a TE reflected wave with orthogonal y-direction electric field to the TM incident wave. As shown in Fig. 2(a), the PRAMC structure has two TM reflection zeros ($f_1 = 2.52$GHz and $f_2 = 3.28$GHz) where the TM reflected wave is solely suppressed whereas the orthogonal TE component is significantly excited. Thus, the polarization state of the incident wave is almost rotated 90° at the two frequency points, which are also named as the polarization-rotation (PR) frequency points. It is observed that there is a large PR frequency band between the PR points f_1 and f_2, and the PR bandwidth for $|\Gamma_{TM/TM}| < -10$ dB is about 38%. Moreover, the phase at the center frequency point of 2.76GHz is equal to 90°, implying that the TM incident wave lags 90° behind the TE reflected wave. Therefore, the incident and reflected waves with a 90° polarization conversion and 90° phase difference can readily constitute a RHCP wave like the dual-via PRAMC [28]. Moreover, the PR point f_2 can be adjusted by changing the length *cut* of the truncated corners to achieve different PR bandwidths and property. It is observed in Fig. 2(b) that enlarging *cut* would increase f_2 but it has less impact on f_1. For the case when *cut* is 6mm, only one frequency point exists and the polarization-rotation property is obviously weakened. It is because the proposed structure with a small *cut* has a small impedance imbalance and is similar to a conventional square AMC structure. Thus, the polarization-rotation property can be properly adjusted by changing the length *cut*.

In addition, compared with the dual-via PRAMC [28], the corner-cut PRAMC can obtain a larger bandwidth about 38% in a same height about $0.045\lambda_0$; meanwhile, it is more easily to apply the DC-bias signals when combined with varactors.

B. POLARIZATION-RECONFIGURABLE AND FREQUENCY-TUNABLE AMC STRUCTURE BASED ON CORNER-CUT PRAMC STRUCTURE

According to the above analysis of the corner-cut PRAMC, the polarization-rotation property can be properly adjusted by changing the capacitances (which can be determined by the length *cut*) along the diagonal directions. For multi-function applications, varactors are loaded directly along the ± 45° to change the reactances X'_1 and X'_2. By adjusting the values of these varactors, different PR properties can be realized and thus a novel active AMC structure can be obtained, as shown in Fig. 3. The top metal patch is a combination of a four-corner-cut inner patch and four triangles loaded with four varactors. Each varactor is connected across the inner patch and one triangle. To control these varactors, each corner is linked with a DC bias line on the back through a vertical via, while the inner patch is connected with the bottom ground through a grounded via. Here, the varactors are divided into two groups with the values (C_1, C_2) respectively along the −45° and +45° diagonal directions. When applying the DC bias voltages on the DC line 1 and 2 respectively for controlling the varactors with different values (C_1, C_2), the surface capacitance along the two diagonal directions can be separately adjusted, thus realizing the polarization-reconfigurable and frequency-tunable property.

Fig. 4 shows the dyadic reflection coefficients of the active AMC structure in cases of the varactors with different values (C_1, C_2). The polarization-rotation property can be properly adjusted by changing the values of the varactors. Based on the PR property of the corner-cut PRAMC, when the value C_1 is much smaller than C_2, a large difference of the surface capacitance along the two diagonal directions is introduced, just like the corner-cut PRAMC in Fig. 1. Then, as shown in Fig. 4(a), the TM reflected wave is solely suppressed

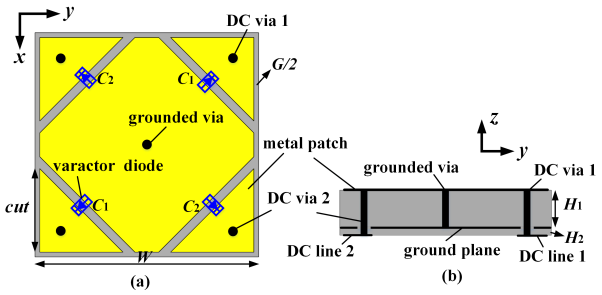

FIGURE 3. The topology of the active AMC structure: (a) top view, and (b) side view. (W = 18 mm, G = 0.2 mm, cut = 8 mm,H_1 =5 mm, H_2 = 0.254 mm).

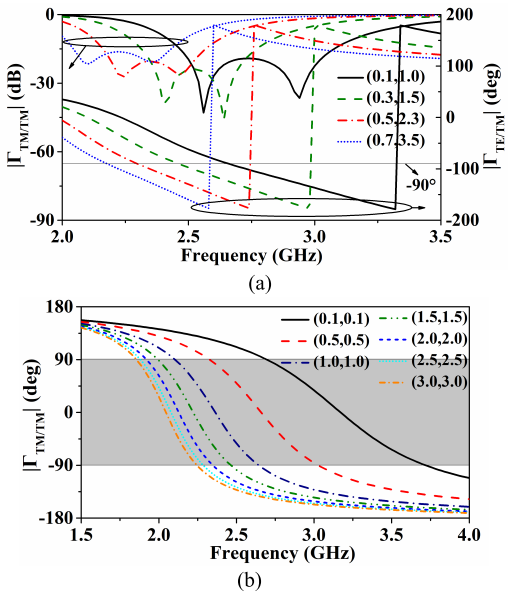

FIGURE 4. The dyadic reflection coefficients of the active AMC structure in cases of the varactors with different values (C_1, C_2): (a) Mode 1 or 2 for CP states, and (b) Mode 3 for LP state.

whereas the orthogonal TE component is significantly excited for achieving 90° polarization rotation. Combing with 90° phase difference between the TM-incident and TE-reflected waves, the LHCP wave is readily obtained. Moreover, the PR band can also be tuned by adjusting the values (C_1, C_2) simultaneously. Here, the PR band can cover 2.01-3.17GHz with a tuning ratio 1.6:1 when the values of the varactors range from 0.1∼3.5pF, as shown in Fig. 4(a). Due to complete symmetry of the active AMC structure, the frequency-tunable RHCP wave can also be achieved when C_2 is much smaller than C_1.

However, when the value C_1 is equal to C_2, the impedances along the two diagonal directions are completely same, thus the AMC structure has no polarization-rotation property but just exhibit in-phase reflection property like the conventional square AMC. Then, the in-phase reflection band (see Fig. 4(b)) can be also adjusted by controlling the values of the varactors, and the band is tunable from 1.85∼3.73 GHz with a tuning ratio 2.0:1 when the values of the varactors range from 0.1∼3pF.

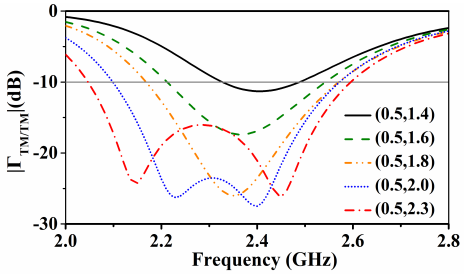

FIGURE 5. The bandwidth-adjustable dyadic reflection coefficients of the active AMC structure in cases of the varactors with different C_2 but C_1 is fixed.

In addition, the PR bandwidth for each CP state can also be adjusted by altering one varactor while fixing another one. As shown in Fig. 5, when C_1 is fixed at 0.5pF and C_2 is changed from 1.4pF to 2.3pF, PR property can also be observed since the value C_1 is much smaller thanC_2. The center frequency is almost unchanged and fixed at about 2.4GHz but the PR bandwidth can be adjusted from 6% to 24%. As listed in Table 1, the performances of the proposed varactor-tuned AMC unit are summarized and the polarization-reconfigurability and frequency-tunability are verified. For further demonstration, the proposed active AMC structure will be applied next to realize one dipole antenna with reconfigurable polarization and tunable frequency.

III. POLARIZATION-RECONFIGURABLE AND FREQUENCY-TUNABLE DIPOLE ANTENNA

A. DESIGN OF ACTIVE AMC-BASED RECONFIGURABLE- AND TUNABLE- DIPOLE ANTENNA

Based on the property of the proposed active AMC structure in Section II, a multi-functional antenna (see Fig. 6) can be designed accordingly by combining one 6 × 6 active AMC structures as the ground plane with a linearly-polarized radiator. Here, the radiator consists of a pair of linearly-polarized dipole antennas (upper dipole 1 and upper dipole 2) with symmetric radiation patterns and is fed by an E-shaped feedline to achieve better impedance matching, as shown in Fig. 6(c)-(d). The dipole antenna is etched on a dielectric slab of Arlon DiClad 880 (ε_r = 2.2, $tan\ \delta$ = 0.0009). As the antenna substrate is placed above the proposed active AMC plane with a small distance H_3, four mounting posts are loaded for supporting the antenna substrate. In addition, a single-layer DC-bias circuit (see Fig. 6(e)-(f)) is also designed for controlling the varactors, which is located on the back of the ground to reduce the effects on antenna. To simplify the DC-bias circuit, the DC line 1 and 2 (marked in red and yellow) of each unit are respectively assembled to the DC port 1 and 2 near the corners, while the negative terminals on the ground plane are guided to the edges on the DC-bias layer by grounded vias. Among them, two positive DC lines are separated by the bridges to avoid signal touch. Note that all the DC lines from each unit are connected with an inductor of 270nH (marked in green) served as a RF-choke to block RF leakage onto the bias lines. Here, for investigating the

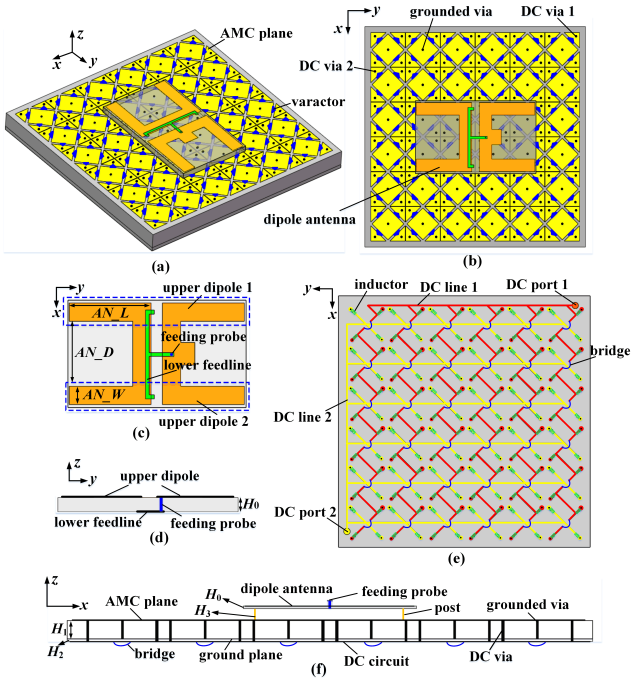

FIGURE 6. Topology of the proposed antenna using active AMC: (a) 3D view, (b) top view, (c-d) zoom-in views of the dipoles, (e) bottom view of DC-bias circuit, and (f) side view. (The optimized geometrical parameters: $H_0 = 0.762$mm, $H_1 = 5$mm, $H_2 = 0.254$mm, $H_3 = 0.5$mm, $W = 18$mm, $G = 0.2$mm, $cut = 8$mm, $AN_L = 29$mm, $AN_W = 6.5$mm, $AN_D = 23$mm).

TABLE 1. Polarization-reconfigurable and frequency-tunable property of the active AMC structure.

Section	Polarization state	Varactors with values (C_1, C_2)	PR band for Mode1 or 2 /in-phase reflection band for Mode3	Band-adjustable
Mode 1	LHCP ($C_1 < C_2$)	Min：(0.1, 1.0)	2.41-3.17 GHz (27.3%)	Yes (0~38%)
		Max：(0.7, 3.5)	2.01-2.49 GHz (21.3%)	
Mode 2	RHCP ($C_1 > C_2$)	Min：(1.0, 0.1)	2.41-3.17 GHz (27.3%)	Yes (0~38%)
		Max：(3.5, 0.7)	2.01-2.49 GHz (21.3%)	
Mode 3	LP ($C_1 = C_2$)	Min：(0.1, 0.1)	2.69-3.73 GHz (32.3%)	No
		Max：(3.0, 3.0)	1.85-2.25 GHz (19.5%)	

approximate limitation of the tuning range of the proposed antenna, the varactor capacitances range from 0.5pF to 9.6pF.

B. POLARIZATION-RECONFIGURABLE CAPABILITY

The switch principle between the LP and CP states of the active AMC structure has been explained in Section II. Here, the polarization states of the proposed antenna using the active AMC structure are also investigated in Figs. 7-11. Similarly, when $C_1 << C_2$, LHCP radiation can be obtained (named as Case I), as shown in Fig. 7 (a). The 3-dB AR bandwidth (ARBW) can reach 10.8%, which is narrower than the impedance band (see Fig. 7(b)) but totally overlapped. In addition, a stable LHCP gain response along the z-axis with a variation of less than 1dB is achieved throughout the whole band and the peak gain is about 8.26dBi at 2.34GHz. Besides, the AR curves and radiation patterns are also symmetric

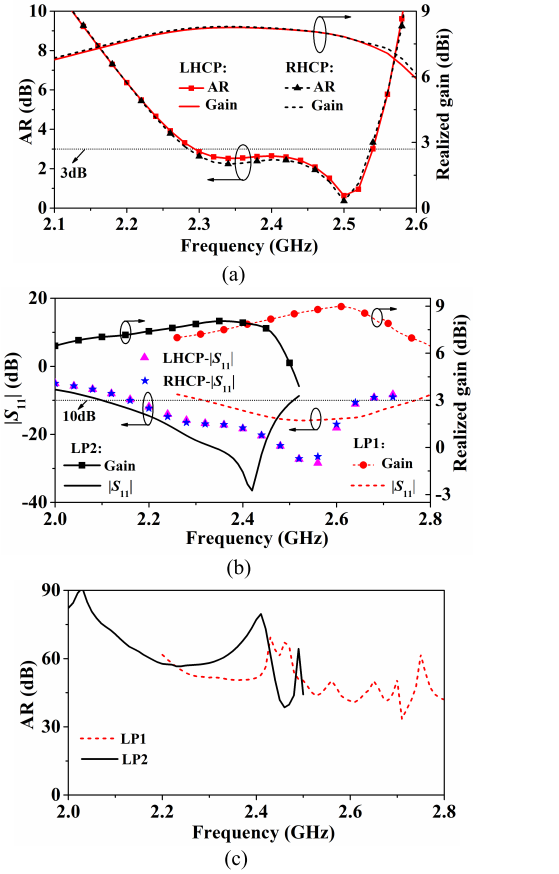

FIGURE 7. Simulated results of the proposed antenna: (a) ARs and gains for LHCP/ RHCP states (b) S parameters for all states and gains for LP states, and (c) ARs for LP states.

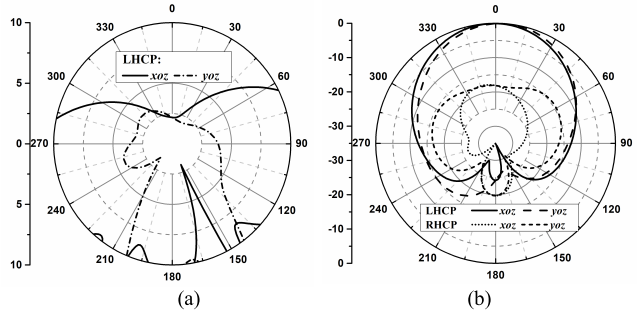

FIGURE 8. Simulated results of the proposed antenna at Case I (LHCP state). (a) ARs versus elevation angle at 2.35GHz and (b) radiation patterns at 2.35GHz.

(see Fig. 8), which respectively show very large 3-dB AR beamwidths of 100° in *xoz* plane and 55° in *yoz* plane and good suppression level of RHCP polarization above 15dB in both the *xoz* and *yoz* plane. Therefore, the proposed antenna can achieve one operation mode with a good broadside LHCP radiation. Conversely, as the proposed antenna is symmetrical, a RHCP radiation (Case II) with same performance can be also obtained by exchanging the value of C_1 and C_2.

As shown in Fig. 7(b)-(c), when $C_1 = C_2$, LP radiations can be obtained since the proposed AMC structure has no polarization-rotation property but just exhibit in-

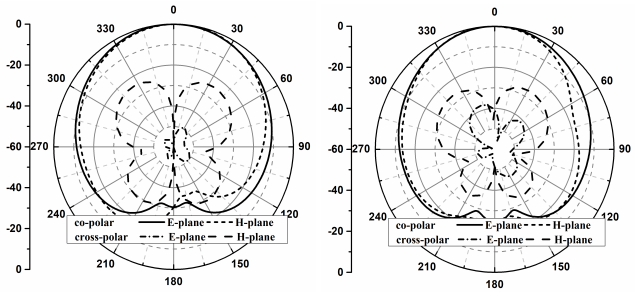

FIGURE 9. Simulated radiation patterns of the proposed antenna at Case III (LP1 state). (a) at 2.45GHz, and (b) at 2.7GHz.

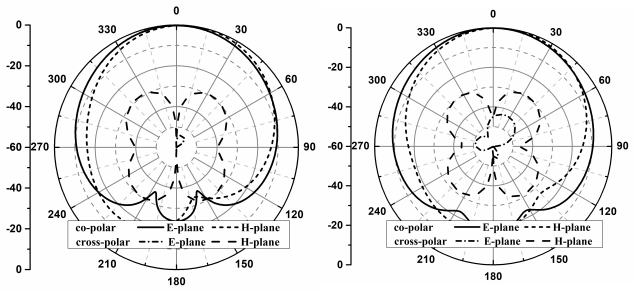

FIGURE 10. Simulated radiation patterns of the proposed antenna at Case IV (LP2 state). (a) at 2.2GHz, and (b) at 2.45GHz.

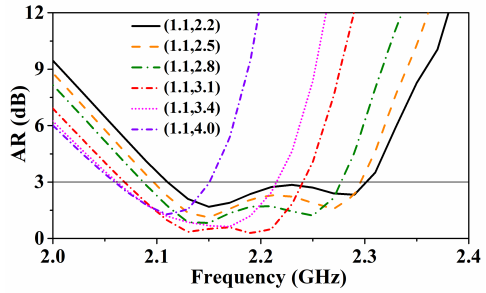

FIGURE 11. Effects on AR curves at CP states when C_1 is fixed to 1.1pF, and C_2 varies.

phase reflection property like the conventional square one. In addition, the operation band can also be tunable if the value C of the varactors is different. Here, two LP states (LP1, LP2) are given, which are respectively named as Case III and IV. As can be seen, the peak gains for the LP1 and LP2 states are respectively 8.97dBi at 2.61GHz and 8.05dBi at 2.36 GHz (see Fig. 7(b)), meanwhile the operation bands respectively range from 2.31∼2.77GHz (18.2%) and 2.09∼2.51GHz (18.3%) correspondingly. Besides, the simulated ARs (see Fig. 7(c)) are larger than 45dB throughout their operation band, indicating very high LP purity. In addition, the radiation patterns of LP1 and LP2 states are also shown in Figs. 9-10, which are symmetric and show very high cross-polarization suppression levels of 25dB in H-plane and 45dB in E-plane. These results for four cases are also listed in Table 2, which demonstrate that the proposed antenna not only exhibits broadband polarization-reconfigurable capability (including a 3-dB ARBW about 10.8% for CP states and a

TABLE 2. Polarization states and their performances of the proposed antenna with different-value varactors.

Case	DC line 1 C_1	DC line 2 C_2	Polarization states	$\|S_{11}\|$<-10dB (GHz)	ARBW (GHz)	Peak gain (dBi)
I	0.5 pF	1.25 pF	LHCP	2.16-2.66 (20.7%)	2.28-2.54 (10.8%)	8.26 (2.34GHz)
II	1.25 pF	0.5 pF	RHCP			
III	0.5 pF (LP1)		LP (frequency tunable)	2.31-2.77 (18.2%)		8.97 (2.61 GHz)
IV	1.25 pF (LP2)			2.09-2.51 (18.3%)		8.05 (2.36 GHz)

10-dB impedance bandwidth about 18.3% for LP states), but also owns good radiation performances for all the polarization states.

Furthermore, we may see that the proposed antenna also owns an ability to tune ARBWs at CP states by varying C_1 and C_2 individually for specific applications. As shown in Fig. 11, when C_1 is fixed to 1.1pF, and C_2 is varied between 2.2 and 4.0pF, the 3-dB ARBW can be tuned from 3.5%∼8.5%. With the continuous increase of C_2, the center frequency of AR is almost unchanged but the bandwidth is decreased. This reveals that the ARBW can be tuned to a certain range by fixing one capacitance and varying another one, which can alter the difference of the surface capacitance along the two diagonal directions.

C. FREQUENCY-TUNING CAPABILITY

Besides the polarization-reconfigurable capability and the 3-dB ARBW-tuning at CP states, the ability of frequency-tuning is another feature of this design. According to the tuning principle of the proposed AMC plane in Section II, the frequency-tunable antenna can be realized by means of tuning C_1 and C_2 simultaneously. Here, the frequency-tuning capability at different polarization states (R/LHCP and LP states) will be discussed in detail.

As described above, the frequency-tuning capability at CP states can be obtained by keeping the large difference and tuning C_1 and C_2 simultaneously. In Fig. 12, the simulated ARs, S_{11} and realized gains versus frequency with different values (C_1, C_2) are given. It is found that good ARs can be realized at arbitrarily selected frequencies between 1.8 and 2.6GHz (see Fig. 12(a)), with a large 3-dB ARBW about 10.8%. Each AR curve is obtained by adjusting C_1 and C_2 to a specific pair of values, which provides flexibility and precision of tuning to achieve satisfactory CP characteristics at any desired frequency within the dynamic range of the varactor. Here, the tunable bandwidth for AR< 3dB can reach about 35% (1.79-2.54GHz) in total with a tuning ratio about 1.42:1, which can be enlarged if the varactor with larger dynamic range is selected. In addition, the corresponding 10-dB impedance bandwidth is sufficiently large and the antenna remains good match over the whole 3-dB AR band. The overlapped band for each state has been clarified with different colors (see Fig. 12(b)). Therefore, AR rather than S_{11} is the crucial characteristic to be concerned in the tuning process. In Fig. 12(c), the corresponding realized gains for

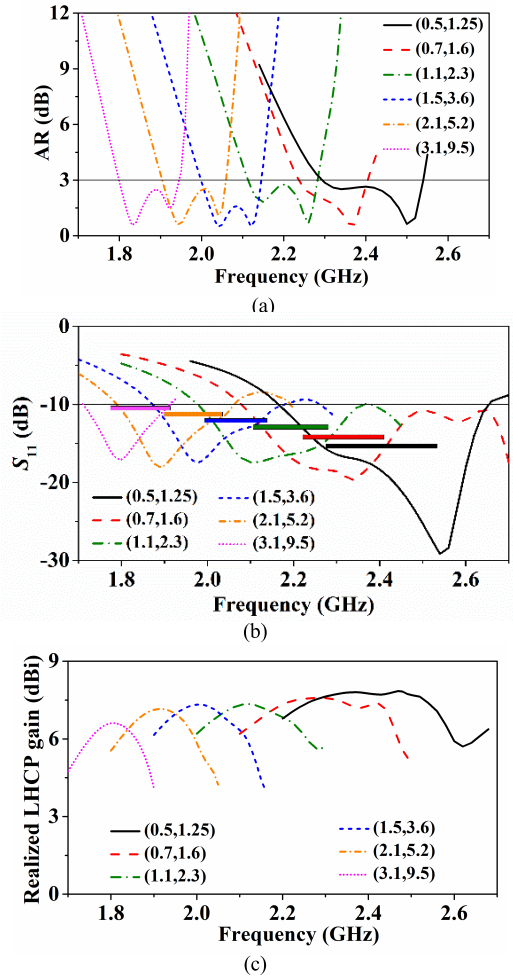

FIGURE 12. Simulated results of the proposed antenna with frequency-tuning capability at LHCP state: (a) ARs (b) *S* parameters, and (c) realized LHCP gain.

LHCP are also given, verifying the frequency-tuning capability at LHCP states.

Similarly, the operation frequency for LP states can also be tunable by keeping C_1 equal to C_2 and changing them to different values. The tunable capability at LP states can be observed in Fig. 13. As we can see, the operating frequency (for $S_{11} < -10$dB) can be arbitrarily selected between 1.5 to 3GHz, with a large 10-dB IMBW about 19%. These curves will move towards low frequency with the capacitance increasing from 0.5 pF to 9.6 pF, thus the proposed antenna can be tuned to any desired frequency within the dynamic range of the varactor. Here, the tunable bandwidth of the operation frequency can reach about 49% (1.72-2.82GHz) in total with a tuning ratio about 1.64:1, which can be enlarged if the varactor with larger dynamic range is selected. Besides, the corresponding realized gains are shown in Fig. 13(b), verifying the frequency-tuning capability at LP states.

To sum up, the tuning characteristics of different polarization states are listed in Table 3. Here, the Case A∼F correspond to the CP states in Fig. 12, while Case G∼L

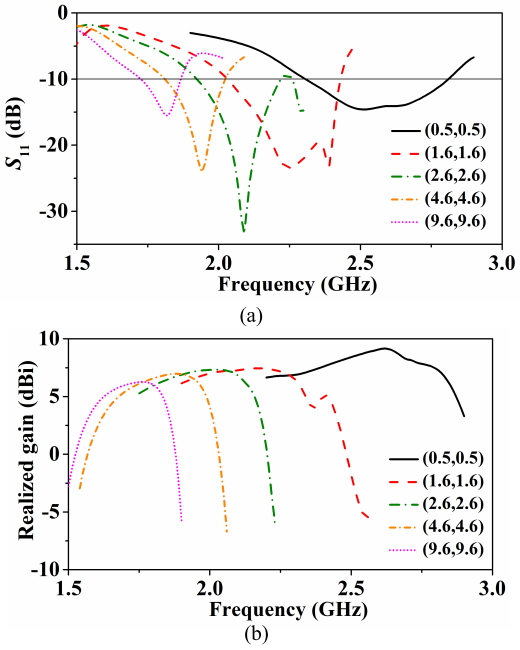

FIGURE 13. Simulated results of the proposed antenna with frequency-tuning capability at LP state: (a) *S* parameters, and (b) realized gain.

TABLE 3. Tuning characteristics Of different polarization states.

	C_1(pF)	C_2(pF)	Freq (GHz)	ARBW(CP) /IMBW(LP)	Polarization
Case A	0.5	1.25	2.41	10.8%	LHCP
Case A*	1.25	0.5	2.41	10.8%	RHCP
Case B	0.7	1.6	2.32	7.3%	LHCP
Case B*	1.6	0.7	2.32	7.3%	RHCP
Case C	1.1	2.3	2.19	7.8%	LHCP
Case D	1.5	3.6	2.07	7.2%	LHCP
Case E	2.1	5.2	1.98	7.9%	LHCP
Case F	3.1	9.5	1.87	7.9%	LHCP
Case G	0.5	0.5	2.54	18.3%	LP
Case H	1.6	1.6	2.23	18.2%	LP
Case I	2.6	2.6	2.07	15.2%	LP
Case J	3.6	3.6	1.98	13.6%	LP
Case K	4.6	4.6	1.92	12.5%	LP
Case L	9.6	9.6	1.80	8.8%	LP

correspond to the LP states in Fig. 13. Thereinto, Case A* and B* were simulated by repeating Case A and B in turn but swapping C_1 and C_2 in each case. Apparently, Case A, A* and Case G show the switches between LHCP, RHCP and LP states, verifying the polarization reconfigurability. In addition, Case A∼F and Case G∼L respectively show the frequency-tuning at different polarization states. Specially, the ARBW of the CP state can reach about 10.8%, which is much wider than other works in [25]–[27] and can satisfy the requirement of large channel capacity in contemporary communication systems. Furthermore, the IMBW of the LP state can be up to 18.3%. Generally speaking, these results demonstrate that the antenna can not only achieve good RHCP, LHCP and LP radiations, but also be easily tuned within the working band for each state.

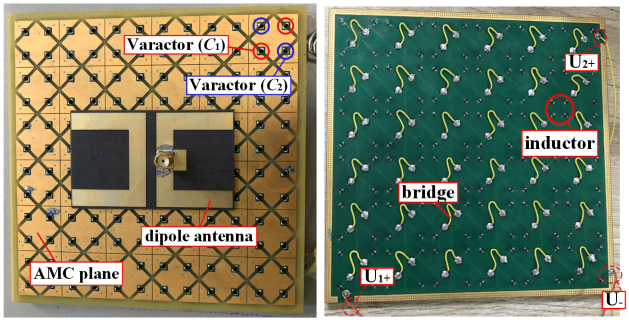

FIGURE 14. Photographs of the fabricated polarization-reconfigurable and frequency-tunable antenna: (a) on the front, and (b) on the bottom.

TABLE 4. Tuning characteristics Of different measured cases with SMV1231.

	U_1(v)	U_2(v)	Freq (GHz)	AR/IMBW	Polarization
Case 1	10	2	2.29	8.7%	LHCP
Case 1*	2	10	2.29	8.7%	RHCP
Case 2	5	1	2.16	7.9%	LHCP
Case 3	2	0	2.00	8.0%	LHCP
Case 3*	0	2	2.00	8.0%	RHCP
Case 4	10	10	2.46	17.1%	LP
Case 5	5.2	5.2	2.34	16.7%	LP
Case 6	1.65	1.65	2.14	16.8%	LP
Case 7	0	0	1.95	15.4%	LP

IV. EXPERIMENTS AND RESULTS DISCUSSION

For further demonstration, the proposed antenna was fabricated by using multi-layer Printed Circuit Board (PCB) technology and the prototype is shown in Fig. 14. Surface mount varactors (SMV1231 with SC-79 package [29]) are soldered on the AMC surface, while the dipole antenna is placed above. On the bottom layer, there are two positive DC ports denoted by (U_{1+}, U_{2+}), respectively controlling the varactors (C_1, C_2) on the AMC plane, while the negative DC port denoted by U_- is linked with 0V as the DC ground. To reduce the effects of the biasing lines on the antenna performance and block the RF energy, an inductor (LQG15HS with an inductance of 270nH from Murata) is loaded on each DC biasing line. In the measurement, the voltages of the two positive DC ports are independently tuned by using two DC power supplies with the range of 0-30V and a precision of 0.01V. In addition, the *S* parameters were measured by the Vector Network Analyzer (VNA), and the radiation performances of this proposed antenna including gains, AR, and the radiation patterns were measured in an anechoic chamber.

The measured results are shown in Figs. 15-18 and listed in Table 4. In Fig. 15(a), the ARs for LHCP state were measured, and the antenna was tuned to exhibit good AR values at three randomly chosen frequencies between 1.8 and 2.6 GHz, respectively. The three curves (Case 1∼3) are listed in Table 4, and their voltage supplies in measurement are also provided. The 3-dB ARBW of each case is 8.7%, 7.9%, and 8.0%, respectively. Owing to the capability of precise tuning over the entire frequency band, the tuning bandwidth for AR< 3dB can reach about 24.1% in total with a tuning

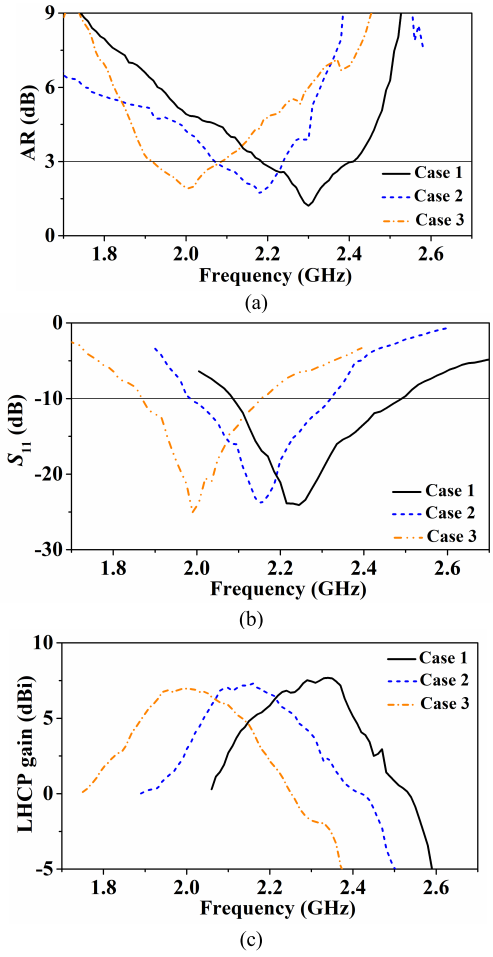

FIGURE 15. Measured results of the proposed antenna with tuning capability at LHCP state: (a) ARs (b) *S* parameters, and (c) LHCP gains.

ratio about 1.28:1, which is little narrower than the simulated results. Specifically, the highest operating frequency has a little drift towards lower frequency compared with simulation, which is mainly caused by the growing capacitance of the varactors vs. frequency together with slight parasitic effects. When biased by the same voltage, the practical capacitances at the frequencies of interest were a little higher than those provided in the datasheet [29] at 1MHz, resulting in lower working frequencies than expected in the simulation. Moreover, the measured S_{11} and LHCP gain for these cases are also shown in Fig. 15(b)-(c), where the tunable performances versus frequency are found. But the measured gains of the three cases exhibit small decreases of about 0.3∼0.7dB due to inevitable losses caused by the varactors with internal resistances and the SMA connector, etc. These results indicate that the proposed antenna exhibits good tuning capability at CP state.

In Fig. 16, the measured results of the fabricated antenna show the tuning capability at LP state by giving four curves (Case 4∼7). These cases are also listed in Table 4, and their voltage supplies in measurement are also provided. The −10dB IMBW of each case is basically more than 15%,

TABLE 5. Comparison with previously reported multi-reconfigurable antennas.

Antenna Type		Polarization-Reconfigurable Capability	Frequency-Tuning capability	Tunable Freq. Range		Height	-10dB IMBW	3-dB ARBW	Band-adjustable	Peak gain (dBi)		Efficiency	Number
				LP	CP					CP	LP		
Network	Patch antenna with switch-based network [17]	LP-V, LP-H, L/RHCP	LP, CP	1.72:1	1.36:1	$0.03\lambda_0$	~5%	--	No	0~3.5	-9~3.5	~30%	1MEMS SPDTS +4Varactors
Patch	Single-fed patch antenna [30]	LP-V, LP-H, LP-±45°	LP	1.4:1	/	$0.02\lambda_0$	~2%	--	No	/	-2.6~6.4	--	4PIN +8Varactors
	Stub-loaded patch Antenna [31]	LP-V, LP-H, LP-45°, L/RHCP	LP, CP	1.43:1	1.5:1	$0.02\lambda_0$	<1%	<0.96%	No	2~8.1	2.6~7.3	~88%	12 Varactors
Slot	Cavity-backed slot antenna [18]	LP-V, LP-H, L/RHCP	LP, CP	1.05:1	1.02:1	$0.01\lambda_0$	3.5%	<1%	No	4~5	4~5	~49%	8PIN
ME dipole	ME-dipole antenna [5]	LP-V, LP-H, L/RHCP	LP	1.24:1	/	$0.25\lambda_0$	~15%	3.6%	No	~8.2	~8.8	~70%	8PIN
Metamaterial-based	EBG-based monopole antenna [25]	LP L/RHCP	CP	/	1.49:1	$0.05\lambda_0$	--	<3.5%	No	--	--	--	112 Varactors
	AMC-based end-loaded dipoles [26]	LP-Arbitray L/RHCP	CP	/	1.22:1	$0.15\lambda_0$	--	<3%	No	4~5	--	--	300 Varactors
	Patch and parasitic pix surface [27]	LP-V, LP-H, L/RHCP	LP	1.29:1	/	$0.07\lambda_0$	2.8%	--	No	--	4~7	~45%	60PIN
	AMC-based dipole antenna using varactors (this work)	**LP, L/RHCP**	**LP, CP**	**1.56:1**	**1.28:1**	**$0.04\lambda_0$**	**17.1 %**	**8.7%**	**Yes (CP)**	**6.6~8.3**	**6.3~9**	**~80%**	**144 Varactors**

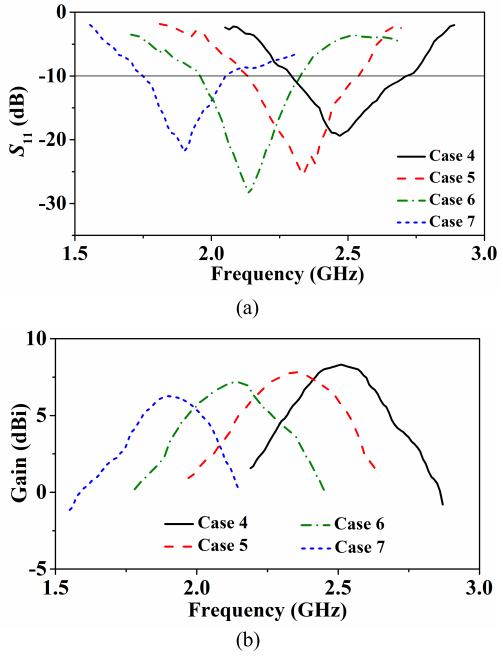

FIGURE 16. Measured results of the proposed antenna with tuning capability at LP state: (a) *S* parameters, and (b) realized gains.

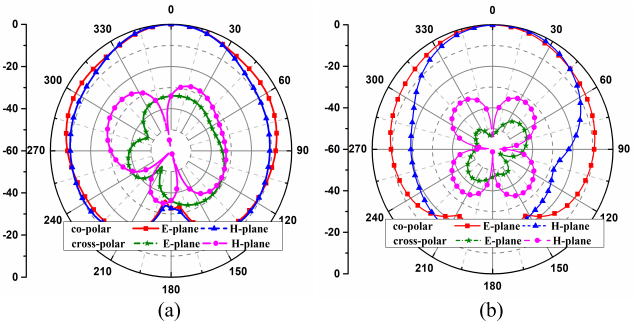

FIGURE 17. Measured radiation patterns of the proposed antenna at LP states: (a) at 2.45GHz for Case 5, and (b) at 2.3GHz for Case 6.

which are respectively 17.1%, 16.7%, 16.8%, and 15.4%. The measured tuning frequency ranges from 1.75 to 2.73GHz with a large tuning ratio about 1.56:1. Similarly, the measured gain has a little attenuation about 0.3∼0.7dB due to the losses of the varactors. In addition, the measured radiation patterns at LP states are also given (see Fig. 17), where the cross-polarization suppression levels are over 25dB. These results indicate that the proposed antenna exhibits good tuning capability at LP state.

To verify the polarization reconfigurability of the proposed antenna, Case 1* and 3* represent two situations in the measurement by repeating Case 1 and 3 in turn but swapping U_{1+} and U_{2+} in each case. The AR and S_{11} curves versus frequency are shown in Fig. 18. Although small differences are observed due to the asymmetry and misalignment in fabrication and measurement, good agreement between the original cases and the star cases can still be obtained, especially near the CP operating frequencies. Thus, these results indicate that the proposed antenna exhibits good polarization reconfigurability.

In summary, the frequency tuning and polarization reconfigurability of the proposed dipole antenna integrated with the varactor-based active AMC plane has been verified efficiently by both simulations and measurements.

To demonstrate the usefulness and advantages of our design, comparisons of the figure-of-merits with previously reported multi-reconfigurable antennas are summarized in Table 5. These common approaches based on slot antennas [18] and patch antennas [30], [31] are simpler, but bandwidths are much smaller (<5%), which is difficult to be enlarged and satisfy the large channel capacity requirement of the modern communications. In contrast, a ME dipole

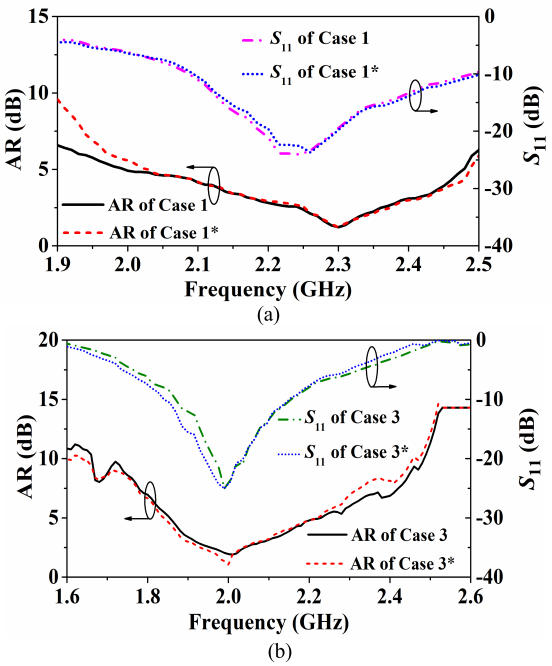

FIGURE 18. Comparison of the measured AR and S_{11} of the proposed antenna to show polarization reconfigurability on switched cases: (a) Case 1 and Case 1*. (b) Case 3 and Case 3*.

antenna [5] can achieve larger bandwidth of 15%, whereas only two or three tuning bands are realized and it requires a relatively larger height of $0.25\lambda_0$. In addition, some designs with switch-based feeding networks [17] are also presented, but these works are too complicated and result in large losses. For metamaterial-based antennas [25]–[27], a large tuning range in a low-profile size can be readily obtained, but the 3-dB bandwidth at single CP state is very small ($< 5\%$) and many important performances are not mentioned. However, in this work, the tunable bandwidth of three polarization states including L/RHCP and LP states can realize large tuning ratios in a low-profile with a high efficiency; meanwhile, the working bandwidth of each tuning state of the antenna is relatively large, i.e. the ARBW of CP states can be up to 8.7% and the IMBW of LP states can approach 17%. Thus, the proposed broadband multi-functional antenna with promising advantages would be a preferable candidate for the applications in modern communication systems to meet the demands of high data rate and large capacity.

V. CONCLUSIONS

In this paper, a polarization-reconfigurable and frequency-tunable dipole antenna using the varactor-based active AMC plane is proposed. The design strategies of the multi-functional antenna and the active AMC structure are described in detail. By controlling the DC bias of the varactors accordingly, not only three polarization states of RHCP, LHCP and LP can be obtained, but also tunable operating frequency of each polarization can be realized. The measured tuning frequency ratio is 1.56:1 ($|S_{11}| < -10$dB) for LP states and 1.28:1 (AR$<$ 3dB) for either LHCP or RHCP. The bandwidth of single polarization state can also be adjusted, and for some LP states or CP states, it can be up to 17.1% and 8.7% respectively. Good polarization-reconfigurability and frequency-tuning capability are demonstrated from the simulated and measured results. The proposed mechanism is believed to be useful for many operational and in-development global navigation systems, including GPS, GLONASS, COMPASS, Galileo, and IRNSS.

REFERENCES

[1] L. Ge and K.-M. Luk, "A band-reconfigurable antenna based on directed dipole," *IEEE Trans. Antennas Propag.*, vol. 62, no. 1, pp. 64–71, Jan. 2014.
[2] I. Lim and S. Lim, "Monopole-like and boresight pattern reconfigurable antenna," *IEEE Trans. Antennas Propag.*, vol. 62, no. 12, pp. 5854–5859, Dec. 2013.
[3] T. J. Jung, I. J. Hyeon, C. W. Baek, and S. Lim, "Circular/linear polarization reconfigurable antenna on simplified RF-MEMS packaging platform in K-band," *IEEE Trans. Antennas Propag.*, vol. 60, no. 11, pp. 5039–5045, Nov. 2012.
[4] H. A. Majid, M. K. A. Rahim, M. R. Hamid, and M. F. Ismail, "Frequency and pattern reconfigurable slot antenna," *IEEE Trans. Antennas Propag.*, vol. 62, no. 10, pp. 5339–5343, Oct. 2014.
[5] F. Wu and K. M. Luk, "Single-port reconfigurable magneto-electric dipole antenna with quad-polarization diversity," *IEEE Trans. Antennas Propag.*, vol. 65, no. 5, pp. 2289–2296, May 2017.
[6] H. Sun and S. Sun, "A novel reconfigurable feeding network for quad-polarization-agile antenna design," *IEEE Trans. Antenna Propag.*, vol. 64, no. 1, pp. 311–316, Jan. 2016.
[7] I. F. Akyildiz, W.-Y. Lee, M. C. Vuran, and S. Mohanty, "NeXt generation/dynamic spectrum access/cognitive radio wireless networks: A survey," *Comput. Netw.*, vol. 50, pp. 2127–2159, Sep. 2006.
[8] M. K. Fries, M. Grani, and R. Vahldieck, "A reconfigurable slot antenna with switchable polarization," *IEEE Microw. Wireless Compon. Lett.*, vol. 13, no. 11, pp. 490–492, Nov. 2003.
[9] P.-Y. Qin, A. R. Weily, Y. J. Guo, and C.-H. Liang, "Polarization reconfigurable U-slot patch antenna," *IEEE Trans. Antennas Propag.*, vol. 58, no. 10, pp. 3383–3388, Oct. 2010.
[10] Y. Sung, "Investigation into the polarization of asymmetrical-feed triangular microstrip antennas and its application to reconfigurable antennas," *IEEE Trans. Antennas Propag.*, vol. 58, no. 4, pp. 1039–1046, Apr. 2010.
[11] R.-H. Chen and J.-S. Row, "Single-fed microstrip patch antenna with switchable polarization," *IEEE Trans. Antenna Propag.*, vol. 56, no. 4, pp. 922–926, Apr. 2008.
[12] W.-S. Yoon, S.-M. Han, J.-W. Baik, S. Pyo, J. Lee, and Y.-S. Kim, "Crossed dipole antenna with switchable circular polarisation sense," *Electron. Lett.*, vol. 45, no. 14, pp. 717–718, Jul. 2009.
[13] F. Ferrero, C. Luxey, R. Staraj, G. Jacquemod, M. Yedlin, and V. Fusco, "A novel quad-polarization agile patch antenna," *IEEE Trans. Antennas Propag.*, vol. 57, no. 5, pp. 1563–1567, May 2009.
[14] L.-Y. Ji, P.-Y. Qin, Y. J. Guo, C. Ding, G. Fu, and S.-X. Gong, "A wideband polarization reconfigurable antenna with partially reflective surface," *IEEE Trans. Antenna Propag.*, vol. 64, no. 10, pp. 4534–4538, Oct. 2016.
[15] K. X. Wang and H. Wong, "A reconfigurable CP/LP antenna with cross-probe feed," *IEEE Antennas Wireless Propag. Lett.*, vol. 16, pp. 669–672, 2017.
[16] M. R. Hamid, P. Gardner, P. S. Hall, and F. Ghanem, "Switched-band Vivaldi antenna," *IEEE Trans. Antennas Propag.*, vol. 59, no. 5, pp. 1472–1480, May 2011.
[17] K. M.-J. Ho and G. M. Rebeiz, "A 0.9–1.5 GHz microstrip antenna with full polarization diversity and frequency agility," *IEEE Trans. Antennas Propag.*, vol. 62, no. 5, pp. 33–40, May 2014.
[18] L. Ge, Y. Li, J. Wang, and C.-Y.-D. Sim, "A low-profile reconfigurable cavity-backed slot antenna with frequency, polarization, and radiation pattern agility," *IEEE Trans. Antenna Propag.*, vol. 65, no. 5, pp. 2182–2189, May 2017.
[19] F. Yang and Y. Rahmat-Samii, "Reflection phase characterizations of the EBG ground plane for low profile wire antenna applications," *IEEE Trans. Antennas Propag.*, vol. 51, no. 10, pp. 2691–2703, Oct. 2003.

[20] F. Yang and Y. Rahmat-Samii, "Microstrip antennas integrated with electromagnetic band-gap (EBG) structures: A low mutual coupling design for array applications," *IEEE Trans. Antennas Propag.*, vol. 51, no. 10, pp. 2936–2946, Oct. 2003.
[21] H. L. Zhu, S. W. Cheung, X. H. Liu, and T. I. Yuk, "Design of polarization reconfigurable antenna using metasurface," *IEEE Trans. Antennas Propag.*, vol. 62, no. 6, pp. 2891–2898, Jun. 2014.
[22] W. Yang, W. Che, H. Jin, W. Feng, and Q. Xue, "A polarization-reconfigurable dipole antenna using polarization rotation AMC structure," *IEEE Trans. Antenna Propag.*, vol. 63, no. 12, pp. 5305–5315, Dec. 2015.
[23] F. Costa, A. Monorchio, S. Talarico, and F. M. Valeri, "An active high-impedance surface for low-profile tunable and steerable antennas," *IEEE Antennas Wireless Propag. Lett.*, vol. 7, pp. 676–680, 2008.
[24] D. Cure, T. M. Weller, and F. A. Miranda, "Study of a low-profile 2.4-GHz planar dipole antenna using a high-impedance surface with 1-D varactor tuning," *IEEE Trans. Antennas Propag.*, vol. 61, no. 2, pp. 506–515, Feb. 2013.
[25] B. Liang, B. Sanz-Izquierdo, E. A. Parker, and J. C. Batchelor, "A frequency and polarization reconfigurable circularly polarized antenna using active EBG structure for satellite navigation," *IEEE Trans. Antennas Propag.*, vol. 63, no. 1, pp. 33–40, Jan. 2015.
[26] C. P. Scarborough, D. H. Werner, and D. E. Wolfe, "Compact low-profile tunable metasurface-enabled antenna with near-arbitrary polarization," *IEEE Trans. Antennas Propag.*, vol. 64, no. 7, pp. 2775–2783, Jul. 2016.
[27] D. Rodrigo, B. A. Cetiner, and L. Jofre, "Frequency, radiation pattern and polarization reconfigurable antenna using a parasitic pixel layer," *IEEE Trans. Antennas Propag.*, vol. 62, no. 6, pp. 3422–3427, Jun. 2014.
[28] W. Yang, K. W. Tam, W. W. Choi, W. Che, and H. T. Hui, "Novel polarization rotation technique based on an artificial magnetic conductor and its application in a low-profile circular polarization antenna," *IEEE Trans. Antennas Propag.*, vol. 62, no. 12, pp. 6206–6216, Dec. 2014.
[29] Skyworks Solutions. (Aug. 2015). *SMV123x_Series: 0.1-10.0GHz Hyperabrupt Junction Tuning Varactors*. [Online].Available: http://www.skyworksinc.com/uploads/documents/SMV123x_Series_2000058X.pdf
[30] P.-Y. Qin, Y. J. Guo, Y. Cai, E. Dutkiewicz, and C.-H. Liang, "A reconfigurable antenna with frequency and polarization agility," *IEEE Antennas Wireless Propag. Lett.*, vol. 10, pp. 1373–1376, 2011.
[31] N. Nguyen-Trong, L. Hall, and C. Fumeaux, "A frequency- and polarization-reconfigurable stub-Loaded microstrip patch antenna," *IEEE Trans. Antennas Propag.*, vol. 63, no. 11, pp. 5235–5240, Nov. 2015.

DONGXU CHEN was born in Xuzhou, Jiangsu, China, in 1994. She received the B.Eng. degree from the Nanjing University of Science and Technology (NUST), Nanjing, China, in 2015, where she is currently pursuing the Ph.D. degree with the Department of Communication Engineering.

In 2017, she was an Exchange Student with the Department of Electronics Engineering, Chang Gung University (CGU). Her main research interests include novel artificial material-based antenna arrays and multi-functional antennas.

She was a recipient of the Best Paper Prize of 2015 Asia Pacific Microwave Conference, in 2015, and the Merit Paper Prize of 2016 International Symposium on InfoComm & Media Technology in Bio-Medical & Healthcare Application, in 2016, Singapore. She serves as a reviewer of IEEE Access, and the IEEE Antennas and Wireless Propagation Letters.

WANCHEN YANG (M'15) was born in Xuzhou, Jiangsu, China, in 1988. She received the B.Eng. degree in communication engineering from Hohai University (HHU), Nanjing, China, in 2010, and the Ph.D. degree in electromagnetic field and microwave technology from the Nanjing University of Science and Technology (NUST), Nanjing, China, in 2015.

From 2013 to 2014, she was a Research Assistant with the University of Macau. In 2017, she was a Postdoctoral Fellow with the City University of Hong Kong. From 2015 to 2018, she was an Assistant Professor with the Nanjing University of Science and Technology. In 2019, she joined the South China University of Technology, Guangzhou, China, where she is currently an Associate Professor. She has authored or coauthored over 60 internationally refereed journal and conference papers, including 20 Transaction papers. Her main research interests include novel artificial material-based antenna arrays, multi-functional antenna arrays, millimeter-wave antenna arrays, and MIMO antenna arrays and technologies.

She was a recipient of the Best Paper Prize of 2014 Student Paper Competition in IEEE HK AP/MTT Postgraduate Conference, in 2014, and the co-recipient of the Best Paper Prize of 2015 Asia Pacific Microwave Conference, in 2015, and the 2017 Outstanding Doctoral Dissertation of Jiangsu Province, China. She serves as an Associate Editor of IEEE Access, and a Reviewer of the IEEE Transactions on Antennas and Propagation, the IEEE Transactions on Microwave Theory and Techniques, the IEEE Transactions on Industrial Electronics, the IEEE Antennas and Wireless Propagation Letters, IEEE Access, the *IET Microwaves Antennas and Propagation*, the *IET Electronic Letters*, and the *Journal of Electromagnetic Waves and Applications*.

WENQUAN CHE (M'01–SM'11) received the B.Sc. degree from the East China Institute of Science and Technology, Nanjing, China, in 1990, the M.Sc. degree from the Nanjing University of Science and Technology (NUST), Nanjing, China, in 1995, and the Ph.D. degree from the City University of Hong Kong (CITYU), Hong Kong, in 2003.

In 1999, she joined the City University of Hong Kong, as a Research Assistant, where she was a Research Fellow and a Visiting Professor, from 2005 to 2006 and 2009 to 2011. In 2002, she joined Polytechnique Montréal, Montréal, QC, Canada, as a Visiting Scholar. From 2007 to 2008, she was with the Institute of High Frequency Technology, Technische Universität München, Munich, Germany. In 2008, she was a Professor with the Nanjing University of Science and Technology. In 2018, she joined the South China University of Technology, Guangzhou, China, where she is currently a Professor. She has authored or coauthored over 300 internationally refereed journal papers and international conference papers. Her research interests include electromagnetic computation, planar/coplanar circuits and subsystems in RF/microwave frequency, microwave monolithic integrated circuits (MMICs), and medical application of microwave technology.

Dr. Che is a member of the IEEE MTT-S AdCom Committee (2018–2020). She was a recipient of the 2007 Humboldt Research Fellowship presented by the Alexander von Humboldt Foundation of Germany, the 5th China Young Female Scientists Award, in 2008, and the Distinguished Young Scientist Award from the National Natural Science Foundation Committee (NSFC) of China, in 2012. She is the Editor of the *Microwave and Optical Technology Letters*, the Associate Editor of the *IEEE Journal of Electromagnetics, RF, and Microwaves in Medicine and Biology*, and a reviewer of the IEEE Transactions on Microwave Theory and Techniques, the IEEE Transactions on Antennas and Propagation, the IEEE Transactions on Industrial Electronics, and the IEEE Microwave and Wireless Components Letters.

QUAN XUE (M'02–SM'04–F'11) received the B.S., M.S., and Ph.D. degrees in electronic engineering from the University of Electronic Science and Technology of China (UESTC), Chengdu, China, in 1988, 1991, and 1993, respectively.

In 1993, he joined UESTC as a Lecturer, and became a Professor, in 1997. From 1997 to 1998, he was a Research Associate and then a Research Fellow with the Chinese University of Hong Kong, Hong Kong. In 1999, he joined the City University of Hong Kong, Hong Kong, where he was a Chair Professor of microwave engineering. From 2011 to 2015, he served the University as the Associate Vice President for Innovation Advancement and China Office, the Director for the Information and Communication Technology Center, and the Deputy Director for the State Key Laboratory of Millimeter Waves, Hong Kong. In 2017, he joined the South China University of Technology, Guangzhou, China, where he is currently a Professor and also the Dean of the School of Electronic and Information Engineering. He has authored or coauthored over 300 internationally refereed journal papers and over 130 international conference papers. He is a Co-Inventor of five granted Chinese patents and 15 granted U.S. patents, in addition with 26 field patents. His current research interests include microwave/millimeterwave/ terahertz passive components, active components, antenna, microwave monolithic integrated circuits, and radio frequency integrated circuits.

Dr. Xue was a recipient of the 2017 H. A. Wheeler Applications Prize Paper Award. He served for the IEEE as an AdCom Member of MTT-S, from 2011 to 2013, an Associate Editor for the IEEE TRANSACTIONS ON MICROWAVE THEORY AND TECHNIQUES, from 2010 to 2013, the Editor for the *International Journal of Antennas and Propagation*, from 2010 to 2013, and the Associate Editor for the IEEE TRANSACTIONS ON INDUSTRIAL ELECTRONICS, from 2010 to 2015. Since 2016, he has been an Associate Editor of the IEEE TRANSACTIONS ON ANTENNAS AND PROPAGATION.

LIZHENG GU was born in Lianyungang, Jiangsu, China, in 1995. He received the B.Eng. degree in communication engineering from the Nanjing University of Science and Technology (NUST), Nanjing, China, in 2016, where he is currently pursuing the Ph.D. degree in electronic science and technology.

His current research interests include metasurface antennas, base-station antennas, and MIMO antenna arrays and technologies.